Journal of Sustainable Metallurgy
https://doi.org/10.1007/s40831-023-00688-z

RESEARCH ARTICLE

CO_2-Minimized Ferrochrome Production Utilizing Silicon Wafer Cutting Slurry as an Alternative Reductant

Marcus Sommerfeld[1] · **Joao Weiss**[1] · **Bernd Friedrich**[1]

Received: 20 December 2022 / Accepted: 18 April 2023

Abstract

Direct emissions due to the use of carbon-based fossil-reducing agents contribute to the overall CO_2 emissions of pyrometallurgical production processes. This study investigated the replacement of fossil coke by silicon-rich cutting waste from the solar wafer cutting process to produce ferrochrome in an electric arc furnace. Laboratory test work and thermochemical simulation were carried out to examine the product quality at various additions of cutting waste and lime. The experimental trials resulted in products in accord with international standards, however, adjusting the slag composition by the addition of lime was necessary, otherwise high silicon contents in the alloys were obtained. Due to the highly exothermic reaction of silicon with iron- and chromium oxides, the silicothermic reduction results in a decreased specific electric energy consumption compared to the carbothermic reduction according to the thermochemical simulation. Low phosphorus and sulfur contents in the alloy might result in premium prices, aiding the economic viability of the process.

Graphical Abstract

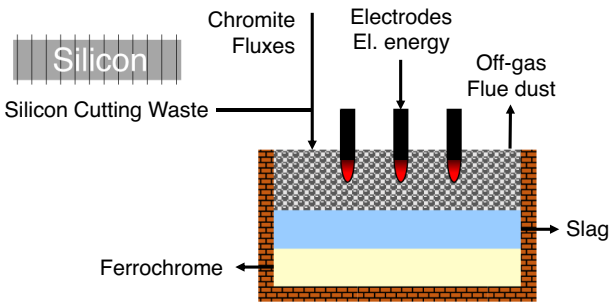

Keywords Ferroalloys · Silicon cutting waste · Alternative reducing agent · Silicothermic reduction · Submerged arc furnace · Electric arc furnace

Introduction

In 2020 12.7 million tons of ferrochrome were produced worldwide [1], an increase of 500% compared to 40 years ago [2]. Thereby, the production of stainless steel has also significantly increased, which particularly reflects the consumption of ferrochrome and raw materials for its production [1]. To produce ferrochrome, different processes have been established, mostly taking place in electric furnaces. Electric furnaces have a simple operation compared with blast furnaces. For example, the use of reducing agents is cheaper and the yield is higher [3]. The demand for ferrochrome is

The contributing editor for this article was Sharif Jahanshahi.

Marcus Sommerfeld and Joao Weiss have contributed equally to this work.

✉ Marcus Sommerfeld
msommerfeld@ime-aachen.de

[1] IME Process Metallurgy and Metal Recycling, Institute of RWTH Aachen University, Intzestraße 3, 52056 Aachen, Germany

Published online: 03 May 2023

expected to increase significantly in the next decade [4]. This directly implies a high demand for feed materials, including fossil carbon as a reducing agent. To produce high-carbon ferrochrome, chromite ore or concentrates, fluxing agents, production metal scraps, and carbonaceous reducing agents like coke, semi-coke, and gas coal are used [5].

Since ferrochrome is conventionally produced using coke as a reducing agent, the smelting process generates a large amount of CO_2. For 2016 it was estimated that the generic CO_2 emissions due to the usage of fossil-reducing agents were 15.5 million tons in ferrochrome production. Since the same options to reduce greenhouse gas emissions might be transferable for other ferroalloys as well, the emissions could increase to 39.1 million tons, if ferromanganese and silicomanganese are included [6]. The replacement of fossil-reducing agents is one step to make the production of ferroalloys more sustainable. Viable options could include the use of bio-based carbon or metallic residues which act as reducing agents. The replacement of hydrogen for the production of ferroalloys seems to be difficult since chromium is less noble than hydrogen [6].

This study aims to minimize CO_2 emissions contributing to carbon-reduced metallurgy, and achieve circular economy through the use of an industrial residue, which can be used as a reducing agent for primary ferrochrome production. The article investigates the use of cutting waste slurry (kerf) from the wafering process of solar cell production. During this production step, approximately half of the high-purity silicon is lost through suspension in this slurry [7]. The slurry contains silicon carbide as a cutting auxiliary, polyethylene glycol (PEG) as a lubricant, metallic silicon, silicon oxide and small amounts of iron and other metallic impurities from the saw wire process. This slurry contains the residue at the end of the wafering process.

A lot of research has been carried out on the recycling of Si and SiC particles from the slurry. Processes have been designed for the separation of the remaining SiC and Si and the corresponding recovery of solar-grade silicon [8]. According to Wang et al. [8] the recovery of pure silicon from kerf was investigated by chemical and physical treatment using a centrifuge, followed by temperature treatment, washing, drying, and finally directional solidification. Through these processes, silicon and silicon carbide components were concentrated and consequently separated.

Pyrometallurgical processes have also been carried out to treat kerf. One method is the recovery of the solar silicon by carbothermic reduction in a submerged arc furnace. After acid leaching or washing of the material, the dried material was mixed with quartz sand and binder and pelletized [9]. Subsequently, the pellets were melted in a direct current electric arc furnace, to produce high-purity silicon. According to Liu et al. [9], a silicon yield of 60% was achieved. Although many methods have been proposed, most are toxic or difficult to be scaled up for industrial production. Despite that, research has also been carried out to utilize the metallic silicon content in kerf as a reducing agent for metallurgical processes [10–12].

The use of kerf instead of coke as a reducing agent in the production of high-carbon ferrochrome may be advantageous to lower the sulfur content in metal, which is an impurity element for ferroalloys. In high-carbon ferrochrome production, most of the sulfur input comes from coke [13]. In addition, it seems feasible to lower the electric energy consumption due to the replacement of coke with kerf. Figure 1 shows the change of standard enthalpy for the reduction of chromium oxide and iron oxide using carbon, silicon carbide, and silicon as reducing agents.

While the carbothermic reductions are endothermic reactions, the reduction with silicon is exothermic. The reduction of chromium oxide by silicon carbide is endothermic, however, less energy is needed compared to the reaction with carbon. The Gibbs free energy change for those reactions is negative and therefore the reactions are spontaneous as shown in previous studies [10, 11]. While previous studies investigated the pre-reduction of chromite or the reduction at lower temperatures [11, 12], which results in an incomplete metal and slag separation [11], a direct smelting approach is investigated in this paper.

Han et al. [10] carried out smelting trials in an electric arc furnace with a capacity of three tons, where pre-treated kerf (50 wt% Si) with chromium concentrates and lime were alternately charged to produce high-carbon ferrochrome. As reported by Han et al. [10], the pre-treatment aimed to

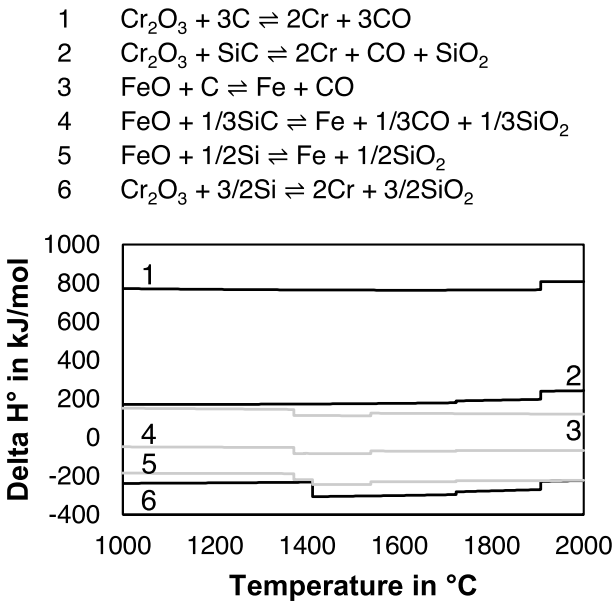

Fig. 1 Change of standard enthalpy of reduction reactions with carbon, silicon carbide, and silicon (data from FactSage™)

remove larger silicon carbide particles. However, this generated ferrochrome with silicon contents above 6 wt%, which does not comply with some standards. Therefore, in this work, a focus was placed on the influence of fluxing and kerf addition on the final product quality.

Materials and Methods

Experimental Setup and Used Equipment

Smelting trials were carried out in a direct current electric arc furnace (EAF) with a voltage up to 80 V and an electrical current up to 1000 A. A graphite crucible with a volume of 2 liters was used for the trials. All trials were carried out with a constant chromite concentrate mass of 2500 g, while the addition of kerf and lime was varied. Two trials were carried out per parameter combination. The raw material was charged manually with a shovel in small batches and heated until the entire raw material was liquid, afterward, the metal and slag were poured into a zirconia-coated cast iron mold. Figure 2 shows a schematic drawing of the furnace and a picture of the furnace during tapping after a trial.

The temperature during the trial was monitored with a digital infrared video thermometer (VIR50, made by Extech Instruments Corporation, Nashua, NH, United States).

To calculate the yield, Eq. (1) is used for the smelting trials, and Eq. (2) is used for the thermochemical simulation. For smelting trials, Eq. (1) is used instead of Eq. (2), since losses due to dusting of chromite concentrate and splashing of slag occur during the laboratory trials, which would not be as significant in an industrial scale. Furthermore, due to the low vapor pressure of chromium, it is not expected that the yield calculation is impaired by volatilization of chromium.

$$\eta_x = 100\% \cdot \frac{m_{x_{\mathrm{Metal}}}}{m_{x_{\mathrm{Metal}}} + m_{x_{\mathrm{Slag}}}} \tag{1}$$

$$\eta_x = 100\% \cdot \frac{m_{x_{\mathrm{Metal}}}}{m_{x_{\mathrm{Input}}}} \tag{2}$$

η_x is the yield of element x; mx_{Metal} is the mass of the element x in the metal; mx_{Slag} is the mass of the element x in the slag; and $m_{x\mathrm{Input}}$ is the mass of element x in the input.

For thermochemical simulation, the equilib, reaction, and phase diagram modules of FactSage™ 8.2 were used [16]. The databases FTmisc, FactPS, and FToxid were selected.

The produced alloys were analyzed with a carbon and sulfur analyzer based on a combustion method (Eltra CS 2000, made by Eltra GmbH, Haan, Germany) and an inductively coupled plasma-optical emission spectrometer (ICP-OES) (Spectro Arcos, made by SPECTRO Analytical Instruments GmbH, Kleve, Germany). The slag was analyzed as fused cast beads with a wavelength dispersive x-ray fluorescence (XRF) spectrometer (Axios$^{\mathrm{mAX}}$, made by Malvern Panalytical B.V., Almelo, Netherlands). The same XRF-spectrometer was used to measure the phosphorus content in ferrochrome.

Kerf was provided by Silicon Processing GmbH, Bautzen, Germany. Excess PEG and water were removed with a filter press to separate a large portion of the liquid material. Kerf was analyzed with the same (ICP-OES) device and carbon and sulfur analyzer as used for the alloy. In addition, the Federov method was used to analyze the metallic silicon content. The Federov method is based on titration. Cupric sulfate, ferric alum, kerf, deionized water and hydrofluoric

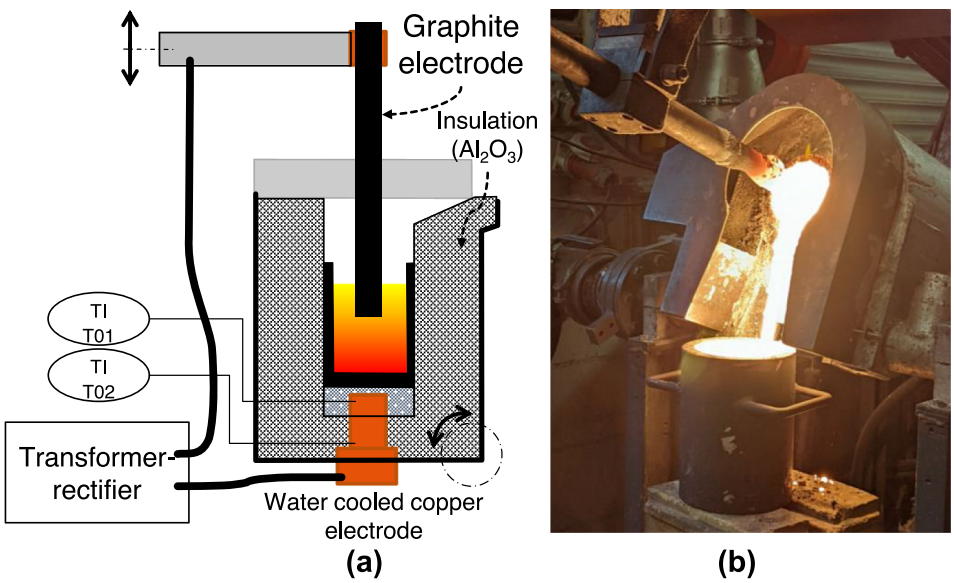

Fig. 2 Schematic drawing of the electric arc furnace (**a**) (after [14, 15]) and tapping of the furnace after a trial (**b**)

acid were heated on a hot plate. Afterward, cold deionized water, sulfuric acid and orthophosphoric acid were added. Excess divalent copper was reduced by metallic silicon to elemental copper, which reduced ferric iron to ferrous iron. The ferrous iron content was measured by redox titration with an indicator using potassium dichromate as a titration agent. The metallic silicon content was calculated based on the used titrant. The titration was carried out using a titrator (888 Titrando made by Metrohm AG, Herisau, Switzerland). Both methods were carried out twice for kerf material. Thermogravimetry of kerf was carried out with a simultaneous thermal analyzer (STA 449 F3 Jupiter® made by Netzsch Gerätebau GmbH, Selb, Germany) under argon atmosphere. The phases present in kerf were analyzed using X-ray powder diffraction (XRD) with a copper anode and a wavelength of 1.540598 Å (STADI P made by STOE&Cie GmbH, Darmstadt, Germany). Highscore Plus was used for evaluating the XRD data and powder diffraction files (PDF) were retrieved from the PDF-4/Axiom database.

The analytical methods which were used to analyze the chromite concentrate are omitted here and described in detail in a previous publication [17].

Materials Used

Table 1 shows the chemical composition of the used chromite concentrate.

The chromite concentrate was sourced from Turkey and contains higher MgO to Al_2O_3 ratios compared to chromite from example South Africa [18]. The MgO to Al_2O_3 ratio is 1.999 on a weight basis and 5.057 on a molar basis.

Figure 3 shows the qualitative XRD analysis of kerf.

According to Fig. 3, the main phase of kerf is silicon (PDF number: 04-001-7247), followed by silicon carbide (PDF number: 04-007-1956), minor peaks can be explained by quartz (PDF number: 04-007-1808) and iron (PDF number: 04-007-9753).

Table 2 shows the directly measured composition of kerf, based on the ICP-OES, C&S, Federov measurements and the mass loss in the thermogravimetric analysis.

Table 1 Composition of the used chromite concentrate (after [17])

Compound	Al_2O_3	CaO	Cr_2O_3	Fe_2O_3
Concentration in wt%	8.503	0.780	48.243	3.756
Compound	FeO	MgO	SiO_2	MnO
Concentration in wt%	10.702	16.997	5.908	0.125
Compound	Na_2O	K_2O	P_2O_5	TiO_2
Concentration in wt%	0.220	0.020	0.006	0.124
Compound	V_2O_5	S	CO_2	H_2O
Concentration in wt%	0.108	0.013	0.529	1.887

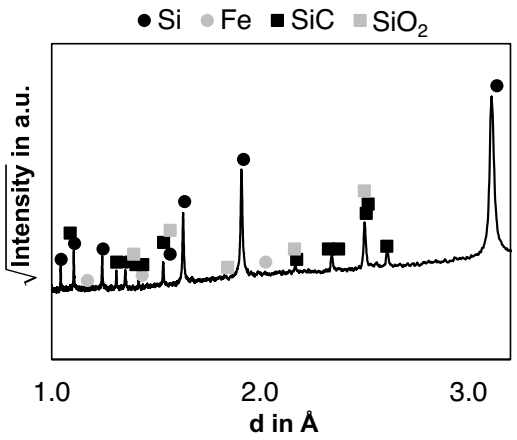

Fig. 3 XRD analysis of kerf

For further evaluation and simulations, an adapted analysis of kerf is used. The mass loss according to Table 2 can be partially attributed to water and PEG, which was assumed to be pure C_2H_4O. The mass loss up to a temperature of 200 °C was assumed to be due to the evaporation of water (15.24 wt%), while the mass loss above 200 °C was attributed to the evaporation of PEG (2.39 wt%). Residual carbon based on Table 2 which cannot be attributed to PEG is allocated to silicon carbide (10.66 wt%). The difference between the total silicon content and the metallic silicon and silicon carbide is attributed to silicon dioxide. Table 3 shows the composition of kerf as used in this study, while the calcium-, iron-, and sodium content are directly taken from Table 2.

Furthermore, kerf was heated in the simulation to 600 °C and only the condensed species were further used in the simulation. In a submerged arc furnace process, the ascending off-gases would pre-heat the charged material before they could react with the melt phase.

Burnt lime (Rheinkalk GmbH, Wülfrath, Germany) with a CaO content of 94.6 wt% was used as a flux. For the simulation and trials, a CaO content of 100 wt% was assumed.

Results and Discussion

Liquidus Temperature of the Slag

To evaluate the liquidus temperature of the slag, a quasi-ternary phase diagram as shown in Fig. 4 was used. Since the chromite concentrate has a molar MgO to Al_2O_3 ratio of 5.057, a $5MgO{\cdot}Al_2O_3$-CaO-SiO_2 phase diagram was used. As a process temperature, 1750 °C was selected. Han et al. [10] suggested, that the process temperature has to be above 1595 °C, to suppress the formation of chromium carbides. In a direct current electric arc furnace, the metal is colder

Table 2 Directly measured composition of the kerf

Ca	Fe	Na	Si_{Met}	Si_{Tot}	C	Δm_{TG}
Value in wt%						
0.315 ± 0.015	4.275 ± 0.175	0.205 ± 0.005	47.10 ± 1.50	63.65 ± 3.75	4.495 ± 0.175	17.63

Table 3 Adapted analysis of kerf for thermochemical simulation (excluding Ca, Fe, Na)

$Si_{Metallic}$	H_2O	C_2H_4O	SiC	SiO_2
Value in wt%				
47.10	15.24	2.39	10.66	19.44

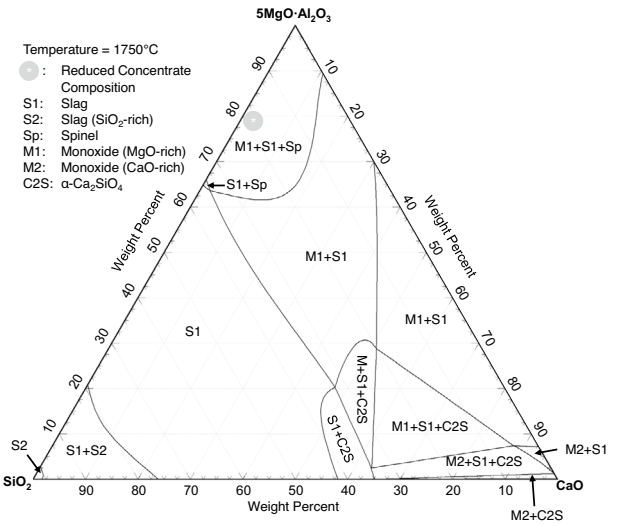

Fig. 4 Predicted phase diagram of the quasi-ternary $5MgO{\cdot}Al_2O_3$, CaO, and SiO_2 slag system at 1750 °C according to FactSage™ [16]

compared to the slag, therefore higher temperatures were selected. Pre-trial testwork showed, that 1750 °C would be a suitable temperature, to obtain a good metal and slag separation after tapping. Lower temperatures might be possible as well, but would increase the necessary amount of fluxes. Therefore, an isothermal phase diagram of the slag at 1750 °C was chosen to identify suitable slag compositions. Since the other main components of the concentrate, chromium oxide and iron oxide were reduced during the trial and transferred to the metal phase, neglecting those elements and the minor components seems to be a justified assumption. The composition of the reduced and simplified concentrate only represented by MgO, Al_2O_3, CaO, and SiO_2 was calculated, and is highlighted in Fig. 4 by an asterisk.

The high melting point of $5MgO{\cdot}Al_2O_3$ (2450 °C [16]) requires a fluxing by SiO_2 or CaO. The liquidus temperature of SiO_2 is 1723 °C [16] and the liquidus temperature of CaO is 2572 °C [16]. The highlighted reduced concentrate has a liquidus temperature of 2227 °C according to FactSage™. As can be seen, the fully reduced concentrate without the addition of other elements lies in a monoxide, spinel, and slag field. To reach the slag field, the addition of SiO_2 is necessary, which is formed when kerf is added due to the silicothermic reaction. For higher SiO_2 additions, it is also possible to add CaO, without leaving the slag phase field. According to the phase diagram, the slag needs to contain around 35 wt% of SiO_2 to be molten at 1750 °C.

It has to be noted, that the phase diagram is only a prediction by a thermochemical simulation software (FactSage™ [16]). Discrepancies in the quaternary system between experimental results and the predictions by FactSage™ have been discussed previously in the literature. Liao et al. [19] investigated the system with a constant weight ratio of 0.4 Al_2O_3/SiO_2. For slags with an MgO content above 15 wt% and a CaO + MgO content above 55 wt%, the predicted liquidus temperature was 105–189 °C higher than the experimental results. The predicted primary phase field in that area was MgO. Similar findings were reported by Yao et al. [20] for the MgO phase field in the Al_2O_3-CaO-SiO_2 slag system containing 5 wt% and 10 wt% MgO in the slag. Especially for slags containing 10 wt% MgO, the liquidus temperature of the experimental slags is at least 100 °C lower compared to the prediction, while the discrepancy becomes smaller if the spinel phase field is approached by increasing the Al_2O_3 content. Wang et al. [21] examined the quaternary system experimentally for a constant CaO/SiO_2 ratio of 0.9 and found a good accordance of isotherms in the spinel phase field. However, the isotherms in the periclase, melilite, olivine and wollastonite phase field differed from the experimental results.

Based on the previous examinations [19–21], it seems that FactSage™ overestimates the liquidus temperature in the MgO-rich area. As a result, the single slag phase field drawn in Fig. 4 might extend more into the MgO-rich monoxide and slag phase field compared to the prediction. This implicates a lower requirement of kerf additions for the envisaged process to maintain a fluid slag. However, the addition of silicon is also a necessity to reduce iron- and chromium oxide.

Ferrochrome Composition

Figure 5 shows the silicon content and carbon content in the produced alloy for various kerf and lime additions according to the trial data and thermochemical model.

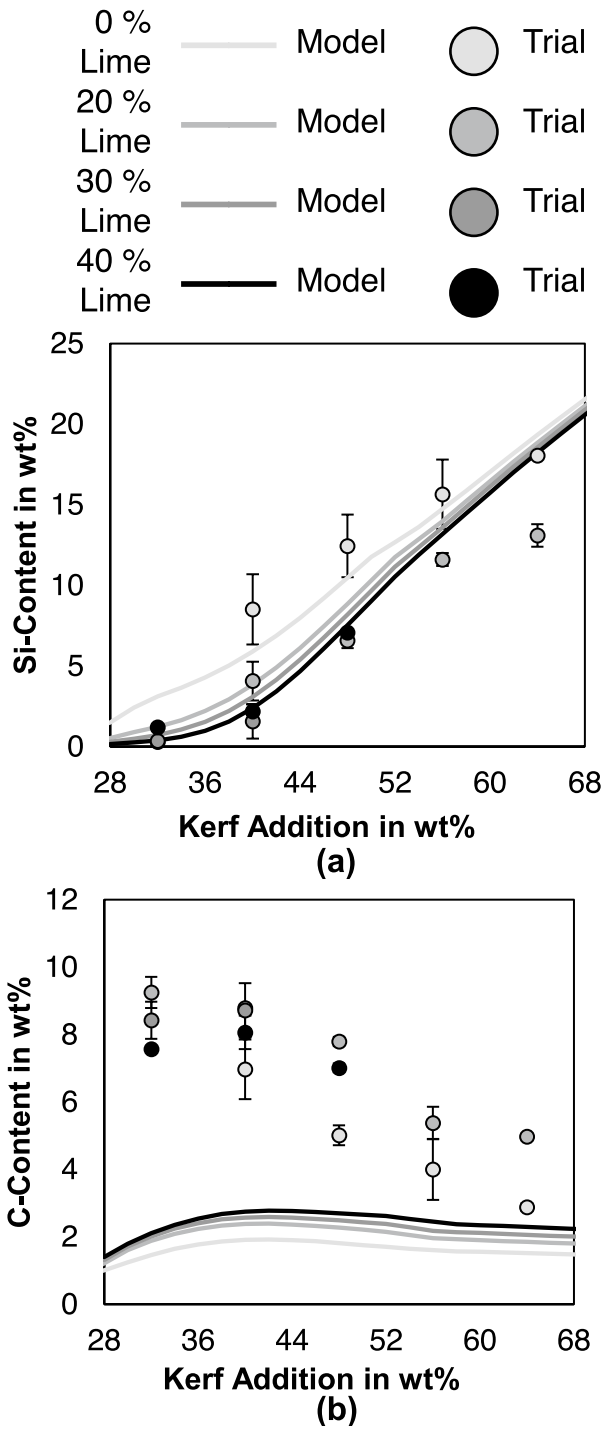

Fig. 5 Silicon (**a**) and carbon (**b**) content in the alloy according to thermochemical model and trial data for different lime and kerf additions at 1750 °C

As shown in Fig. 5, an increasing lime addition decreases the silicon content in the alloy, while an increase in the kerf addition will increase the silicon content in the alloy. Except for the trial series without lime additions and for the trials with a lime addition of 20 wt% for high kerf additions, the trial data and the thermochemical model match fairly well regarding the silicon content. Not all of the produced metal samples were within the limits of standards for ferrochrome. Table 4 shows the limits for carbon and silicon in ferrochrome according to Deutsches Institut für Normung (DIN) and ASTM International (ASTM).

Table 4 Limits for carbon and silicon in ferrochrome according to ASTM and DIN

Element	C	Si
Unit	wt%	wt%
ASTM high carbon A [22]	6–8	< 6.0
ASTM high carbon B [22]	6–8	8.0–14.0
ASTM high carbon C [22]	6–8	< 3.0
DIN suraffiné [23]	< 0.50	< 1.5
DIN affiné [23]	1–2	< 1.5
DIN carburé [23]	6–8	2–5

Only trials with low kerf additions and lime additions above 30 wt% resulted in acceptable products regarding silicon according to the DIN ferrochrome carburé standard and ASTM High Carbon C standard. Lower lime additions or higher kerf additions with lime at least satisfied the ASTM High Carbon A or B standards. However, most samples with a low silicon content were above the carbon limit of 8 wt% for high carbon alloys, therefore further refining for example in a converter seems to be necessary. This might be avoidable if carbon is not used as a smelting vessel, unlike in this study. According to the simulation, it is even possible to meet the DIN ferrochrome affiné standard for low kerf additions and high lime additions with respect to the carbon- and silicon content. However, it is not possible to meet the DIN ferrochrome suraffiné standard, due to the carbon content of kerf.

The trial data does not match the predicted carbon content according to the thermochemical model. While only small deviations can be seen in the carbon content if kerf or lime is varied according to the model, a significant decrease in the carbon content can be seen if the kerf addition is increased. This is probably due to the carbon content in ferrochrome decreasing when the silicon content in the alloy increases. The higher carbon content in the alloy for the trials is explainable by the used graphite crucibles. Since a conductive bottom is necessary for direct current EAFs, a graphite crucible was necessary for the trials. For alternating current furnaces with a refractory lining or a water-cooling and a freeze-lining operation, it might be possible to reduce the uncontrolled carbon input and hence match the carbon values predicted by the thermochemical model. These values are significantly lower than the carbon values in ferrochrome produced via carbothermic reduction.

Table 5 shows the concentration of chromium, iron, and trace elements in the ferrochrome, the mean deviation, and the number of analyzed trials for each element, and the limits stated in the standards. As trace elements, phosphorus and sulfur are shown, because those elements are typical impurities in ferrochrome, furthermore copper is shown since copper can be an impurity in kerf.

According to Table 5, the phosphorus and sulfur content were significantly below the standards, which might result in a price premium for ferrochrome produced with kerf as a reducing agent. The concentration of copper was still within the range. The chromium content was mostly dependent on the kerf addition, since chromium is diluted by silicon in the alloy for higher kerf additions. Nevertheless, most samples were within the chromium ranges, even though trials with high kerf additions did not meet the ASTM High Carbon C standard with respect to the chromium content.

Chromium Yield

Figure 6 shows the chromium yield and the residual chromium content in the slag based on the thermochemical model and the trial data for varying lime and kerf additions.

As shown in Fig. 6, except for high kerf additions, the chromium yield was higher in the trials than in the thermochemical model and the chromium content in the slag was lower. This is explainable by the reaction of the carbon-saturated metal with the slag, which leads to an excess reduction compared to the simulation. The reaction of carbon-saturated metal with oxides was also observed by other authors before [24, 25]. Another explanation might be an overestimation of the SiO_2 content of kerf in Table 3, if more silicon or silicon carbide is present in kerf, the simulation will underestimate the chrome yield.

According to the simulation, increasing the lime addition increases the reduction of chromium, however, this was not proven by the trials, at least for lower kerf additions, higher lime additions did decrease the yield. Only for higher kerf additions, higher yields for higher lime additions were observable. In all cases, the highest yields were only observable, for parameters that resulted in high silicon contents in the alloy as can be seen in Fig. 5.

Specific Electric Energy Consumption

Due to the exothermic reduction of iron and chromium oxides by silicon, it is expected that the specific electric energy consumption (SEC) would be lower compared to the traditional carbothermic reduction process. Since the trial data in a laboratory scale is not representative compared to an industrial operation, Fig. 7 shows the SEC for varying lime and kerf additions based on the thermochemical model per ton of produced alloy and per ton of produced chrome.

As a comparison, the reduction using graphite was also simulated. The graphite input temperature was set to 600 °C, since the same assumption was made for kerf as well. SiO_2 was added as quartz. Since most trials were carried out with a kerf addition of 40 wt% and assuming that the silicon present in kerf as shown in Table 2 completely reacts to SiO_2, 54.46 wt% of quartz were added for the simulation of the carbothermic reduction.

As can be seen in Fig. 7, various lime additions only have a minor impact on energy consumption. While for kerf, the specific energy consumption decreased for increasing additions until a plateau is reached. An increase in the specific energy consumption can be seen for graphite additions above 22.5 wt%. The different behavior can be explainable by the energy-intensive reduction of silicon by graphite, while in the case of kerf a large fraction of silicon is already in the metallic state. Nevertheless, the smelting reduction process using kerf had a significantly lower SEC compared to the carbothermic reduction, while 4587 kWh/t alloy was necessary in the lowest case for the carbothermic reduction, only 1335 kWh/t alloy was necessary in the lowest case for the reduction with kerf. However, the amount of added silica in the carbothermic reduction process was relatively high and literature data reports values of 4200 kWh/t ferrochrome [26], 4500 kWh/t ferrochrome [27], and 3800–4500 kWh/t ferrochrome [28] for ferrochrome production without pre-heating or pre-reduction. Therefore, the model might overestimate the energy

Table 5 Composition of ferrochrome and limits according to ASTM and DIN

Element	Cr	Fe	Cu	P	S
Unit	wt%	wt%	ppm	ppm	ppm
Concentration ± mean deviation	60.0 ± 3.6	27.3 ± 1.9	313 ± 53	45 ± 11	24 ± 13
Number of analyzed trials	32	32	25	17	32
ASTM high carbon A [22]	51–56	–	< 500	< 300	< 400
ASTM high carbon B [22]	56–62	–	< 500	< 300	< 500
ASTM high carbon C [22]	> 62	–	< 500	< 300	< 500
DIN affine [23]	55–75	–	–	< 300	< 500
DIN carburé [23]	45–70	–	–	< 300	< 500

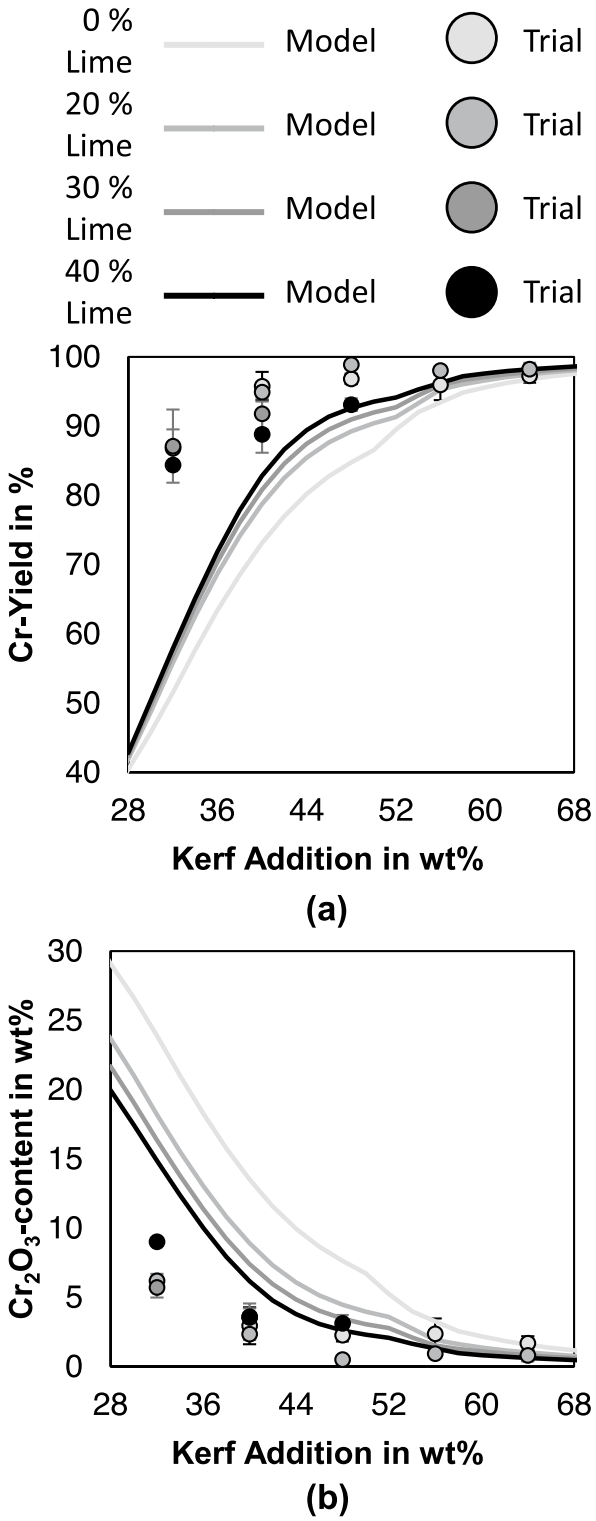

Fig. 6 Chromium yield (**a**) and residual Cr_2O_3 content in the slag (**b**) based on thermochemical simulation and trial data for different lime and kerf additions at 1750 °C

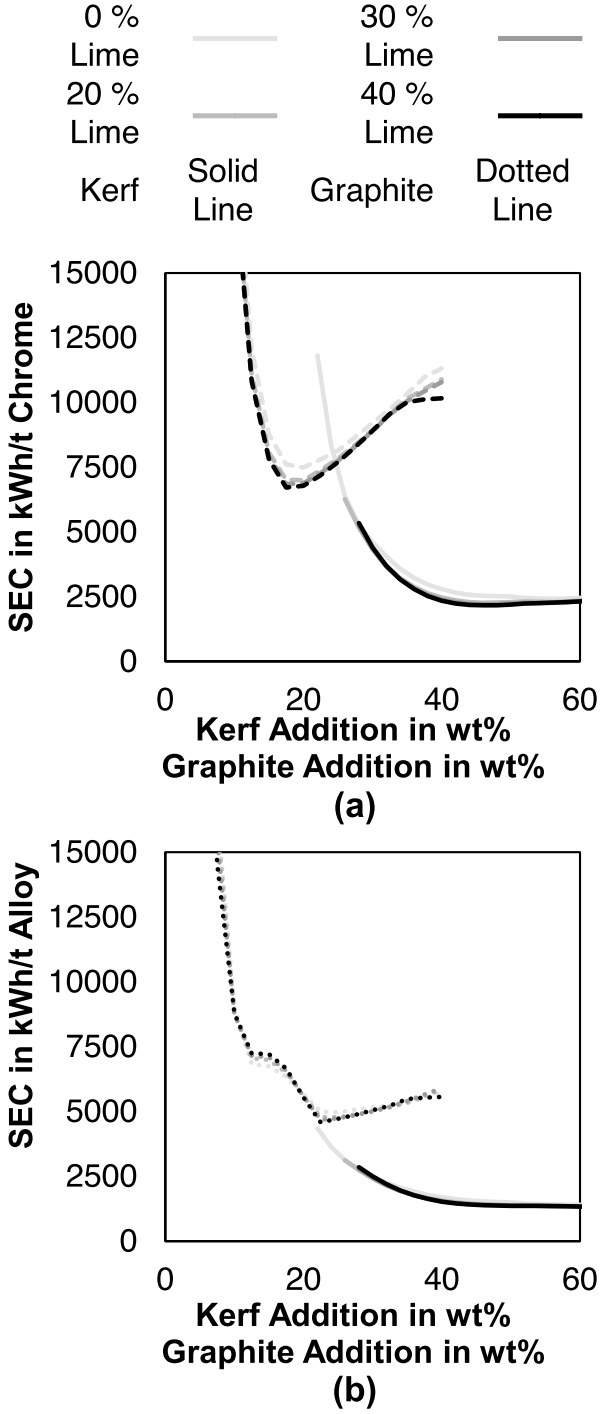

Fig. 7 Specific electric energy consumption per ton of chrome (**a**) and per ton of produced alloy (**b**), according to the thermochemical model for different lime and kerf additions at 1750 °C

consumption of the carbothermic reduction process, due to the high silica addition. Nevertheless, Han et al. reported savings of 50% regarding the energy consumption for trials with an EAF with a capacity of three tons [10].

Conclusion

The usage of silicon cutting waste as an alternative reducing agent to produce ferrochrome according to technical standards proved to be feasible.

Trials with 40 wt% lime addition and 32 wt% kerf addition resulted in a product according to the ASTM High Carbon C standard [22] with 62.4 wt% chromium, 27.2 wt% iron, 7.6 wt% carbon, and 1.2 wt% silicon. Chromium yields were in the range of 86.8–98.9% with an average yield of 93.4%.

Due to reduced amounts of sulfur (24 ppm on average) and phosphorus (45 ppm on average) in the final product, it might be possible to receive a premium on the produced ferrochrome. However, copper concentration in the product was relatively high, although less than standard (313 ppm on average) and must be monitored for the selection of kerf as a reducing agent. Special attention has to be given to the fluxing strategy since the slag will enrich in silica after kerf reacted, fluxing by lime is necessary to control the silicon content in the product. In addition, due to the exothermic silicothermic reduction, it is possible to produce ferrochrome using less electrical energy compared to the traditional carbothermic reduction process while at the same time, less direct CO_2 emissions occur.

Funding Open Access funding enabled and organized by Projekt DEAL. The work did not receive external funding.

Declarations

Conflict of interest The authors report there is no conflict of interest to declare.

References

1. Schulte RF (2022) Chromium [advanced release]. In: U.S. Geological Survey (ed) minerals yearbook 2020. volume I, metals and minerals. US Geological Survey
2. Holappa L, Louhenkilpi S (2013) On the role of ferroalloys in steelmaking. Proceedings of the thirteenth international ferroalloys congress. pp 1083–1090
3. Gasik M (2013) Technology of chromium and its ferroalloys. In: Gasik M (ed) Handbook of ferroalloys. Elsevier, Amsterdam, pp 267–316
4. Pariser HH, Backeberg NR, Masson O et al (2018) Changing nickel and chromium stainless steel markets—a review. J S Afr Inst Min Metall 118:563–568. https://doi.org/10.17159/2411-9717/2018/v118n6a1
5. Gasik M, Dashevskii V, Bizhanov A (2020) Ferroalloys: theory and practice, 1st edn. Springer International Publishing, Cham
6. Sommerfeld M, Friedrich B (2021) Replacing fossil carbon in the production of ferroalloys with a focus on bio-based carbon: a review. Minerals 11:1286. https://doi.org/10.3390/min11111286
7. Lin YC, Wang TY, Lan CW et al (2010) Recovery of silicon powder from kerf loss slurry by centrifugation. Powder Technol 200:216–223. https://doi.org/10.1016/j.powtec.2010.02.028
8. Wang TY, Lin YC, Tai CY et al (2009) Recovery of silicon from kerf loss slurry waste for photovoltaic applications. Prog Photovolt Res Appl 17:155–163. https://doi.org/10.1002/pip.863
9. Liu Y, Kong J, Zhuang Y et al (2019) Recycling high purity silicon from solar grade silicon cutting slurry waste by carbothermic reduction in the electric arc furnace. J Clean Prod 224:709–718. https://doi.org/10.1016/j.jclepro.2019.03.187
10. Han PW, Chen PX, Chu SJ et al (2015) A novel process to produce chromium ferroalloy by use of solar grade crystalline silicon cutting slurry waste. Proceeding of the fourteenth international ferroalloys congress. INFACON, pp 422–428
11. Jung W, Hossain ST, Johra FT et al (2019) Reduction of chromium ore by recycled silicon cutting sludge waste with carbon addition. J Iron Steel Res Int 26:806–817. https://doi.org/10.1007/s42243-018-0195-z
12. Jung WG, Back GS, Johra FT et al (2018) Preliminary reduction of chromium ore using Si sludge generated in silicon wafer manufacturing process. J Min Metall B Metall 54:29–37. https://doi.org/10.2298/JMMB170520054J
13. Dai W, Shu L (1995) On sulfur control in HC FeCr production. Proceedings of the seventh international ferroalloys congress. INFACON, pp 287–296
14. Sommerfeld M, Vonderstein C, Dertmann C et al (2020) A combined pyro- and hydrometallurgical approach to recycle pyrolyzed lithium-ion battery black mass part 1: production of lithium concentrates in an electric arc furnace. Metals 10:1069. https://doi.org/10.3390/met10081069
15. Sommerfeld M, Friedmann D, Kuhn T et al (2018) "Zero-waste": a sustainable approach on pyrometallurgical processing of manganese nodule slags. Minerals 8:544. https://doi.org/10.3390/min8120544
16. Bale CW, Bélisle E, Chartrand P et al (2016) FactSage thermochemical software and databases, 2010–2016. Calphad 54:35–53. https://doi.org/10.1016/j.calphad.2016.05.002
17. Sommerfeld M, Friedrich B (2022) Proposition of a thermogravimetric method to measure the ferrous iron content in metallurgical-grade chromite. Minerals 12:109. https://doi.org/10.3390/min12020109
18. Sweeten NJ, Verryn S, Oberholzer J et al (2018) Chrome ore mineralogy and the furnace mass and energy balance. J S Afr Inst Min Metall. https://doi.org/10.17159/2411-9717/2018/v118n6a12
19. Liao J, Qing G, Zhao B (2023) Phase equilibria studies in the CaO-MgO-Al_2O_3-SiO_2 system with Al_2O_3/SiO_2 weight ratio of 0.4. Metals 13:224. https://doi.org/10.3390/met13020224
20. Yao Z, Ma X, Lyu S (2021) Phase equilibria of the Al_2O_3–CaO–SiO_2-(0%, 5%, 10%) MgO slag system for non-metallic inclusions control. Calphad 72:102227. https://doi.org/10.1016/j.calphad.2020.102227

21. Wang D, Chen M, Jiang Y et al (2020) Phase equilibria studies in the CaO–SiO_2–Al_2O_3–MgO system with CaO/SiO_2 ratio of 0.9. J Am Ceram 103:6651–7321. https://doi.org/10.1111/jace.17421
22. ASTM International (2019) Standard specification for ferrochromium. ASTM
23. Deutsches Institut für Normung (2004) Ferrochrom, ferrochrom-silicium und chrom-technische lieferbedingungen (DIN 17565:2004-02)
24. Philbrook WO, Kirkbride LD (1956) Rate of FeO reduction from a CaO-SiO_2-Al_2O_3 slag by carbon-saturated iron. JOM 8:351–356. https://doi.org/10.1007/BF03377696
25. Sun H, Mori K, Pehlke RD (1993) Reduction rate of SiO_2 in slag by carbon—saturated iron. Metall Mater Trans B 24:113–120. https://doi.org/10.1007/BF02657877
26. Gasik M (ed) (2013). Elsevier, Amsterdam
27. Bergman K, Kjellberg B (2001) DC arc furnace technology applied to smelting applications. Proceedings of the ninth international ferroalloys congress. pp 80–89
28. Holappa L (2010) Toward sustainability in ferroalloys production. Proceedings of the twelfth international ferroalloys congress. pp 1–10